*Journal of Applied Mechanics and Technical Physics, Vol. 37, No. 3, 1996*

# NUMERICAL SOLUTION OF THE PROBLEM OF EJECTION EXPLOSION IN A TWO-LAYER MEDIUM IN A PULSE-HYDRODYNAMIC FORMULATION

**L. V. Gorodilov**

UDC 534.222+622.235

The problem of determining the ejection crater generated by an explosion in a two-layer medium is investigated within the framework of a pulse-hydrodynamic model (its solid–liquid variant) for plane and axial symmetry. The densities and critical velocities determining the ejection crater shape may be different in each layer. We search for the crater boundary numerically by the method of successive approximations using the method of boundary elements in each calculation step. This method has been previously used in calculations of crater profiles in homogeneous media [1–3]. For a two-layer medium, the problem of determining the ejection crater profile in an explosion of a cord charge has been investigated in a solid–liquid formulation using the method of conformal transformations [4–6] for the case of plane symmetry, and the layers were considered to be of the same density.

This paper presents the profiles of craters produced by the action of spherical and infinite cylindrical sources, which simulate an explosive charge, in two-layer media with a strengthless upper layer. The calculation results for the action of spherical sources are compared with the results of experimental explosions of underwater surface explosive charges.

In the solid–liquid formulation of the pulse-hydrodynamic model (PHM) for ejection explosion considered below, the medium is treated as an ideal incompressible liquid only in the region bounded by the crater profile, which is an absolutely rigid wall, within which the medium is at rest [7]. The crater profile is a streamline on which the condition is met that the tangential derivative of the potential is equal to the quantity called the critical velocity.

For a two-layer medium, we can formulate the following boundary-value problem: determine an unknown section $\Gamma_1 + \Gamma_3$ of the boundary $\Gamma$ (Fig. 1) such that the function $\varphi$ satisfies the Laplace equation

$$\Delta\varphi = 0, \tag{1}$$

in the region $\Omega_1 + \Omega_2$, the boundary conditions on $\Gamma$, and the continuity conditions for the normal velocity and pulse pressure at the interface:

$$\partial\varphi_1/\partial s = v_1 \quad \text{on} \quad \Gamma_1; \tag{2a}$$

$$\partial\varphi_1/\partial n = 0 \quad \text{on} \quad \Gamma_1; \tag{2b}$$

$$\partial\varphi_2/\partial s = v_2 \quad \text{on} \quad \Gamma_3; \tag{3a}$$

$$\partial\varphi_2/\partial n = 0 \quad \text{on} \quad \Gamma_3; \tag{3b}$$

$$\rho_1\varphi_1 = \rho_2\varphi_2 \quad \text{on} \quad \Gamma_2; \tag{4}$$

$$\partial\varphi_1/\partial n = -\partial\varphi_2/\partial n \quad \text{on} \quad \Gamma_2; \tag{5}$$

$$\varphi_2 = 0 \quad \text{on} \quad \Gamma_4; \tag{6}$$

$$\varphi_2 = -\varphi_0 \quad \text{on} \quad \Gamma_5. \tag{7}$$

Mining Institute, Siberian Division, Russian Academy of Sciences, Novosibirsk 630091. Translated from Prikladnaya Mekhanika i Tekhnicheskaya Fizika, Vol. 37, No. 3, pp. 67–74, May–June, 1996. Original article submitted April 26, 1994; revision submitted April 18, 1995.

0021-8944/96/3703-0357 $15.00 

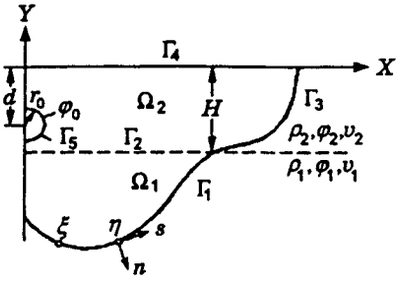


Fig. 1

By virtue of symmetry, Fig. 1 shows only the right-hand side of the crater profile: $X$ and $Y$ are the coordinates; $\Gamma_1 + \Gamma_3$ is the crater boundary; $\Gamma_2$ is the interface; $\Gamma_4$ is the free surface; $\Gamma_5$ is the boundary of the explosive charge; $s$ and $n$ are the arc coordinate and the external normal to the crater boundary; $\varphi_0$ is the potential on the charge boundary; $\rho_1$, $\varphi_1$, and $v_1$ and $\rho_2$, $\varphi_2$, and $v_2$ are the densities, potentials, and velocities of the first and second layers, respectively; $r_0$ is the radius of the pulse source; $H$ is the thickness of the upper layer; $d$ is the distance between the source's center and the free surface; and $\eta$ and $\xi$ are points on the boundary $\Gamma$.

Converting to dimensionless variables in problem (1)–(7), i.e., $x/H$, $y/H$, $\varphi_0/(v_1H)$, $r_0/H$, $v_2/v_1$, $\rho_2/\rho_1$, $d/H$, we can see that for a two-layer medium with plane-parallel boundaries the coordinates $x/H$ and $y/H$ depend on five dimensionless variables: $\overline{\varphi}_0 = \varphi_0/(v_1H)$, $\overline{r}_0 = r_0/H$, $\overline{v}_2 = v_2/v_1$, $\overline{\rho}_2 = \rho_2/\rho_1$, and $\overline{d} = d/H$.

Since part of the boundary is unknown and is to be determined, we are unable to obtain immediately a solution of problem (1)–(7) in the physical domain. Hence, to obtain the unknown boundary of the ejection crater, we use a numerical algorithm that is similar to that of [1–3] and based on the method of successive approximations using the method of boundary elements in each calculation step.

In the first step, the initial boundary $\Gamma_1 + \Gamma_3$ of the crater is specified rather arbitrarily. Mixed boundary-value problem (1)–(7) for the Laplace equation with conditions (2b) and (3b) is solved by the method of boundary elements, and the values of the potential and tangential velocities are found along the boundary $\Gamma_1 + \Gamma_3$ for this configuration of the region $\Omega_1 + \Omega_2$.

The values of the tangential velocities thus obtained are compared with conditions (2a) and (3a), which should be met at the required boundary, and in the case of a difference the boundary of the region is shifted. Then we again solve the boundary-value problem, and so on. We stop the calculations when the difference between the tangential velocities along boundary sections $\Gamma_1$ and $\Gamma_3$ and the given critical velocities $v_1$ and $v_2$ becomes less than 1%. Note that in the case considered below, when the critical velocity in the upper layer is $v_2 = 0$, boundary $\Gamma_3$ does not move and is an extension of the interface.

To solve the Laplace equation, we use the following equation (see, for example, [8]):

$$c(\xi)\varphi(\xi) + \int_\Gamma \varphi(\eta)\, q^*(\xi,\eta)\, d\Gamma(\eta) = \int_\Gamma q(\eta)\, \varphi^*(\xi,\eta)\, d\Gamma(\eta), \tag{8}$$

where $c(\xi)$ is a constant that is equal to $\gamma/\pi$ ($\gamma$ is the solid angle at which surface $\Gamma$ is viewed from point $\xi$); $\varphi(\eta)$ and $q(\eta)$ are the potential and its derivative with respect to the external normal to the region $\Omega$ at point $\eta \in \Gamma$; $\varphi^*(\xi,\eta)$ is a solution of the Laplace equation [for plane symmetry $\varphi^*(\xi,\eta) = -(1/\pi)\ln r(\xi,\eta)$ and for axial symmetry $\varphi^*(\xi,\eta) = 1/(2\pi r(\xi,\eta))$, where $r(\xi,\eta)$ is the distance between points $\xi$ and $\eta$]; $q^* = \partial\varphi^*/\partial n$.

The boundary $\Gamma$ is the contour of a cylindrical surface for plane symmetry and the contour of the generatrix of a rotational surface for axial symmetry. To solve Eq. (8) numerically, we use the Krylov–Bogolybov method [9], which involves the replacement of integral equations by a system of algebraic equations. The boundaries of regions $\Omega_1$ and $\Omega_2$ are divided into almost equal linear sections (boundary elements); $\varphi$ and

$q$ are assumed to be constant in each element and their values are referred to the middles of the sections (nodal points); the elements at the interface coincide. Equation (8) is written in discrete form for each boundary element in regions $\Omega_1$ and $\Omega_2$ and supplemented by conditions (4) and (5). Thus, a completely defined system of linear algebraic equations is obtained.

To find the coefficients (integrands) of the resulting system of linear equations, we use the Simpson quadrature formula for boundary elements with $\eta \neq \xi$ and the analytical expressions of [8] for plane symmetry or the quadrature formula of [10] for axial symmetry (near point $\eta = \xi$) for elements with $\eta = \xi$.

In each iteration, sections $\Gamma_1$ and $\Gamma_3$ are moved in two steps. At first we fix the boundary element that is the nearest to the symmetry axis and then move the other elements, comparing the velocity $v_j$ at each element with the velocity $v_{11}$ at the first element on boundary $\Gamma_1$ and with velocity $v_{22}$ at the interface on boundary $\Gamma_3$. In the process, we move the $j$th element of the boundary along the normal to the element surface at the point of intersection with the $(j+1)$th element by distances

$$\tau_j^1 = l_j k_1 (v_j/v_{11} - 1), \tag{9a}$$

$$\tau_j^2 = l_j k_1 (v_j/v_{22} - 1) \tag{9b}$$

for the first and the second layers, respectively. Here $l_j$ is the half-length of the $j$th element and $k_1$ is specified as a function of $v_{\max}$ [the maximum value of $|v_j - v_{nn}|/v_{nn}$ along the sections $\Gamma_n$ $(n = 1.2)$]. The first two terms of expressions (9) are scale factors; the last specifies the direction and relative magnitude of boundary movement: the required boundaries move along the external normal for $v_j > v_{nn}$ and along the internal one for $v_j < v_{nn}$.

The next iteration begins when $v_{\max} > 0.1$. To approximate the velocity along the required boundaries to the critical velocities for $v_{\max} \leqslant 0.1$, we extend or compress the boundaries of regions $\Omega_1$ and $\Omega_2$ by comparing velocities $v_{11}$ and $v_{22}$ with critical velocities $v_1$ and $v_2$ in each subregion by the following formulas: for the first layer,

$$x_j = x_j v_{11}^{k_2}, \qquad y_j = (y_j + 1)\, v_{11}^{k_2} - 1,$$

and for the second layer,

$$x_j = x_j\, (v_{22}/v_2)^{k_2}, \qquad y_j = (y_j + 1)(v_{22}/v_2)^{k_2} - 1 \qquad (k_2 = 0.1\text{–}0.3).$$

To implement the method, a package of FORTRAN-77 programs has been developed. The run-time of one iteration in calculations of crater profiles on an IBM 360 for $N = 40$ contour points does not exceed 6 sec for the axisymmetric case and 4 sec for the plane case. The prescribed accuracy (1%) is usually attained after 20–30 iterations. A comparison of the crater profiles calculated by the algorithm developed with those found analytically for plane symmetry [6] shows that the maximum relative error in calculations of crater boundaries does not exceed 4% for $N > 50$ contour points.

To verify the method, we calculate craters generated by explosion of underwater surface charges. The calculated results are compared with experimental data on explosions of spherical charges with a mass of 0.2–2.5 g [11, 12]. In this case, the upper layer (water) did not have strength; its critical velocity $v_2 = 0$ and its density $\rho_2 = 1$ g/cm$^3$. The density of the lower layer $\rho_1$ was equal to the density of the material used in the experiments ($\rho_1 = 1.2$ g/cm$^3$ for plasticine and $\rho_1 = 2.6$ g/cm$^3$ for a sand–cement composition [11, 12]). The upper layer thickness $H/r_0$ was varied from 0 to 50 in the calculations.

The first series of profile calculations is performed for craters produced by spherical sources. The pulse pressure on the charge surface is calculated using the approach of [13], according to which the expression for the kinetic energy of an ideal incompressible liquid with an internal pulse source of radius $r_0$ was set equal to the effective part of the total explosion energy $\alpha$ (for sphere, it is 0.4 [14]). From the resulting equation, we found values of the pulse pressure and potential $\varphi_0$ on the surface; the latter was found to be $1.59 \cdot 10^3$ m$^2$/sec for a PETN charge with a density of 1.5 g/cm$^3$ and radius $r_0 = 1$ m. The critical velocity $v_1$ is selected by comparing the depth of the calculated craters with that of experimental craters with upper layer thickness $H/r_0 = 5$. It turned out that, in spite of the substantial difference in the strengths of these materials, the

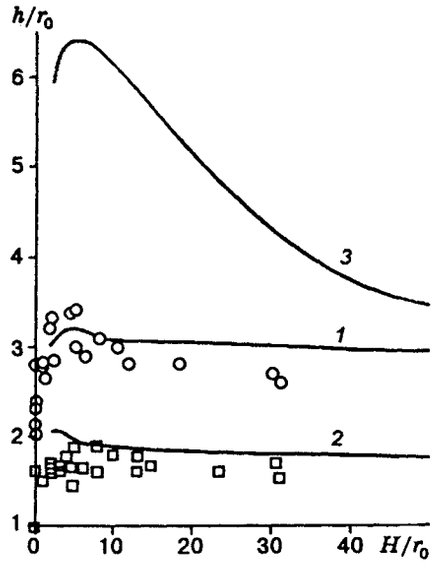


Fig. 2

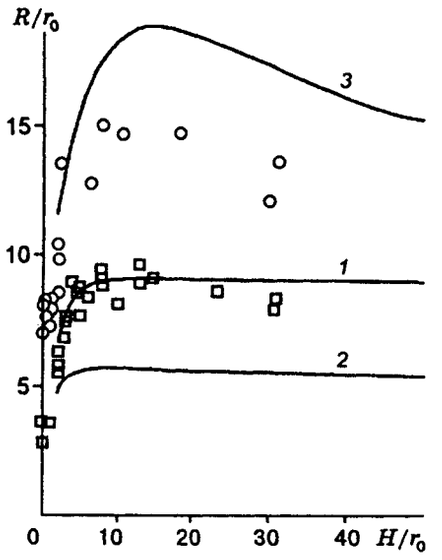


Fig. 3

critical velocities for both the plasticine and sand–cement mixture can be considered equal to 43.4 m/sec. This is apparently connected with the features of explosions of charges of small mass.

In laboratory experiments [11] at a depth of $H/r_0 > 2$–3, crater formation occurred primarily by displacement and compaction of the bottom material without ejection of material. In practice (in explosion of a charge of large mass), craters are generated mainly by ejection of material from the epicenter. It is precisely this mechanism of crater formation that is included in the criterion for determination of crater profile in the solid–liquid formulation of the PHM. We did not change the potential on the source surface and the critical velocity as $H/r_0$ changed.

The craters calculated for pulse sources in a two-layer medium are characterized by a large ejection index $n$ (the crater radius $R$ related to its depth $h$) and the crater edges are horizontally stretched and emerge smoothly on the interface level. When they are compared with the crater profiles calculated for pulse sources in a homogeneous medium (see, e.g., [7]), it is apparent that these two cases are qualitatively different, i.e., the crater in a homogeneous medium is compact and its edges approach the free surface at an angle of $\pi/2$. Similar distinctions are observed in experiments on explosion of surface charges on a free surface and in water, and also with changes in water depth $H/r_0$ [11].

Figures 2–4 present calculated and experimental curves of the crater depths $h$ and radii $R$ referred to the charge radius $r_0$ and of the volume $V$ referred to the charge mass $Q$ versus the depth $H/r_0$ (curves 1 and the circles correspond to the calculation and experiment results, respectively, for $\rho_1 = 1.2$ g/cm$^3$, and curves 2 and the squares, for $\rho_1 = 2.6$ g/cm$^3$). Comparison of the calculated and experimental curves of $h/r_0 = f(H/r_0)$ and $R/r_0 = f(H/r_0)$ shows their qualitative similarity. All the calculated dependences have optima, i.e., values of upper-layer thickness at which the functions have maxima. As in the experiments, an increase in the density of the material of the lower half-space leads to a decrease in the parameters of the calculated craters.

At the same time, for a denser bottom material, the calculated optima fall on a smaller thickness of the upper layer, whereas the experiments show the reverse picture. This apparently results from the fact that the real destruction process of a medium under dynamic loading takes a finite time interval, which is known to increase with increasing strength and density of the material. Hence, for effective crater formation in explosions in a sand–cement mixture, it is necessary to maintain the explosion-product pressure for a longer time interval than in explosions in plasticine. In these experiments, the explosion-pulse duration increases

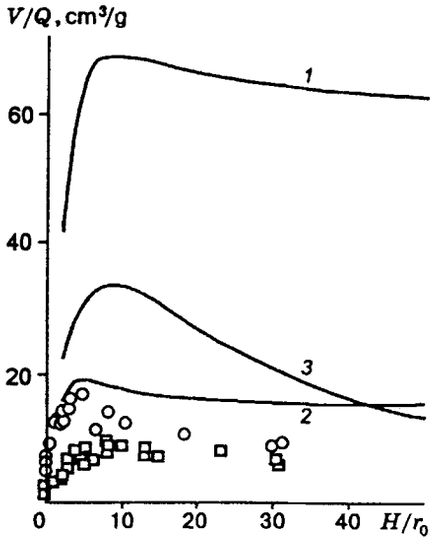


Fig. 4

with increasing water depth and, therefore, for a sand-cement mixture optima occur at a greater depth than for plasticine. This factor is not considered in the PHM, which leads to a discrepancy between calculation and experiment results.

When the critical velocity is such that the calculated crater depths are close to the experimental crater depth in most of the range of upper-layer depth $H/r_0$, the calculated radii are smaller by a factor of $\simeq 1.5$ than those observed in experiments almost everywhere in the range of $H/r_0$ and the volumes are, on the contrary, greater by a factor of $\simeq$ 4–8. In this connection it should be noted that there are some differences between the calculated and experimental crater profiles, namely, the calculated crater has a wider middle base and a taper with an upward-directed vertex, which is typical for the PHM. Moreover, a pronounced effect can be exerted by the discrepancy between crater shaping under an explosion of a small charge and the criterion of crater profile determination included in the PHM, which was mentioned above in choosing the critical velocity. A calculation of the profile of a crater generated by explosion of an underwater surface charge under natural conditions [15] has shown that the discrepancy between the calculated and experimental crater parameters does not exceed 15% in this case.

In blasting practice, extended explosive charges, along with concentrated charges, find wide use in ejection explosions. This paper presents calculations of the action of infinite cylindrical sources, which correspond to underwater explosions of extended surface charges. The results of these calculations are compared with those obtained previously for spherical sources. The critical velocities and densities are $v_1 = 43.4$ m/sec, $v_2 = 0$, $\rho_1 = 1.2$ g/cm$^3$, and $\rho_2 = 1$ g/cm$^3$. For a quantitative comparison of the results, the pulse pressure and potential on the surface of the cylindrical source were calculated in the same way as in the previous series of calculations for the spherical source; in this case we take into account that $\alpha = 0.2$ for the cylindrical source [16]. For a PETN charge with a density of 1.5 g/cm$^3$, the calculated potential on the surface of a cylindrical source of unit radius is $\varphi_0 = 1.86 \cdot 10^3$ m$^2$/sec.

The crater profiles calculated for cylindrical sources and their variation with a change in the upper layer thickness are qualitatively similar to the profiles calculated for spherical sources. Figures 2–4 show the calculated crater parameters versus the thickness of the upper layer for explosions of spherical and cylindrical (curves 1 and 3) charges. For both cylindrical and spherical sources, all crater parameters at certain optimum values of $H/r_0$ have maxima which are more distinct and are attained at large depths.

The linear dimensions of craters (depth $h/r_0$ and radius $R/r_0$) for cylindrical sources are larger than those for spherical sources everywhere in the range of $H/r_0$. In this case the ratio of the crater depths, which is $\simeq 1.9$ for $H/r_0 = 2$–5, decreases with increasing water depth and is $\simeq 1.16$ for $H/r_0 = 50$. The calculated

crater radii for cylindrical sources are larger than those for spherical sources by a factor of 1.7–2 everywhere in the range of $H/r_0$. Conversely, the crater volumes referred to the masses of charges that are equivalent to the corresponding pulse sources are smaller for cylindrical sources than for spherical sources everywhere in the range of $H/r_0$; their ratio is $\simeq 1.93$ for $H/r_0 = 2$ and grows to $\simeq 4$ (for $H/r_0 = 50$) as the upper layer thickness grows.

From a physical viewpoint, these results seem to be rather justified. The energy concentration per unit volume for a cylindrical pulse source is much greater than that for a spherical source, and this explains the fact that in the first case the linear dimensions of the crater ($R/r_0$ and $h/r_0$) are larger than in the second case. At the same time, since the conversion of explosion energy to kinetic energy of the medium is less efficient in explosions of cylindrical charges compared with explosions of spherical ones (this is included in calculations by the coefficient $\alpha$), the explosion efficiency (crater volume $V$) referred to the total explosion energy (charge mass $Q$) in the first case is less than in the second case. As calculations show (Fig. 4), for $H/r_0 = 2$, the ratio $V/Q$ almost coincides with the ratio of the coefficients $\alpha$, which is about 2; with increasing $H/r_0$ this proportion fails and for $H/r_0 = 50$ the ratio for a spherical source is $\simeq 4$ times as large as for a cylindrical source. From this viewpoint, at great water depths, the explosion efficiency is higher for concentrated surface charges than for linear ones.

Thus, the algorithm developed allows us to calculate crater profiles in ejection explosion in two-layer media for linear and concentrated charges in a pulse-hydrodynamic formulation. Here we observe qualitative agreement between calculations and experiments (particularly for soft soils). Within the scope of the PHM, we can try to gain better quantitative agreement with experimental results. For this, the influence of the interface and the free surface on the source (explosive charge) parameters should be taken into account.

## REFERENCES


1. N. B. Il'inskii and A. V. Potashov, *Boundary-Value Problems of Explosion Theory* [in Russian], Izd. Kazansk. Univ., Kazan' (1986).
2. T. B. Borisova, N. B. Il'inskii, and S. E. Khairullin, "Development of the method of boundary integral equations as applied to problems of ejection explosion," in: *Proc. of the Boundary-Value Problems Workshop* [in Russian], No. 20, Izd. Kazansk. Univ., Kazan' (1983).
3. V. K. Krasnov, "Solution of axisymmetric problems of explosions using the method of boundary integral equations," Moscow (1984). Deposited at VINITI 05.07.84, No. 2900–84.
4. E. B. Polyak and E. N. Sher, "The shape of an ejection crater due to the explosion of a cord charge in a two-layer medium," *Zh. Prikl. Mekh. Tekh. Fiz.*, No. 2, 143–146 (1973).
5. N. B. Il'inskii and A. V. Potashov, "Determination of ejection hollow due to the explosion of an underground cord charge in a two-layer medium," *Zh. Prikl. Mekh. Tekh. Fiz.*, No. 2, 109–114 (1978).
6. L. V. Gorodilov and P. A. Martynyuk, "The problem of determining the crater boundary in the underwater explosion of a cylindrical surface explosive charge," *Fiz. Tekh. Probl. Razrab. Polezn. Iskop.*, No. 3, 23–28 (1991).
7. V. M. Kuznetsov, "The shape of an ejection crater due to surface explosions," *Zh. Prikl. Mekh. Tekh. Fiz.*, No. 3, 152–156 (1960).
8. K. Brebbia, J. Telles, and L. Vroubel, *Methods of Boundary Elements* [Russian translation], Mir, Moscow (1987).
9. L. V. Kantorovich and V. I. Krylov, *Approximate Methods of Mathematical Analysis* [in Russian], Gostekhteorizdat, Moscow–Leningrad (1952).
10. V. V. Voinov and O. V. Voinov, "A numerical method of calculation of unsteady flows of an ideal incompressible liquid with free surfaces," *Dokl. Akad. Nauk SSSR*, **221**, No. 3, 559–562 (1975).
11. L. V. Gorodilov and A. P. Sukhotin, "Features of underwater explosions," in: *Collection of Papers on the Problem of Physics of Rocks* [in Russian], Mosk. Gorn. Inst., Moscow (1984).
12. L. V. Gorodilov and A. P. Sukhotin, "The action of explosion of a surface explosive charge on the bottom of a water reservoir," *Fiz. Tekh. Probl. Razrab. Polezn. Iskop.*, No. 4, 110–112 (1987).

13. O. E. Vlasov, *Foundations of Dynamics of Explosions* [in Russian], Izd. Voen.-Inzh. Akad., Moscow (1957).
14. R. Cole, *Underwater Explosions* [Russian translation], Izd. Inostr. Lit., Moscow (1950).
15. V. V. Galkin, R. A. Gil'manov, and I. Z. Drogoveiko, *Underwater Blasting* [in Russian], Nedra, Moscow (1987).
16. V. K. Kedrinskii, "A cylindrial gas cavity pulsating in an unbounded fluid," in: *Dynamics of Continuous Media* [in Russian], Institute of Hydrodynamics, Novosibirsk, **8** (1971), pp. 59–68.